J Mater Sci (2008) 43:6704–6713
DOI 10.1007/s10853-008-2646-6

Mixed-mode crack growth in bonded composite joints under standard and impact-fatigue loading

Ian A. Ashcroft · Juan Pablo Casas-Rodriguez · Vadim V. Silberschmidt

Received: 19 March 2008 / Accepted: 10 April 2008 / Published online: 31 July 2008

Abstract Carbon fibre reinforced polymers (CFRPs) are now well established in many high-performance applications and look set to see increased usage in the future, especially if lower cost manufacturing and solutions to certain technical issues, such as poor out-of-plane strength, can be achieved. A significant question when manufacturing with CFRP is the best joining technique to use, with adhesive bonding and mechanical fastening currently the two most popular methods. It is a common view that mechanical fastening is preferred for thicker sections and adhesive bonding for thinner ones; however, advances in the technology and better understanding of ways to design joints have lead to increasing consideration of adhesive bonding for traditionally mechanically fastened joints. In high-performance applications fatigue loading is likely and in some cases repetitive low-energy impacts, or impact fatigue, can appear in the load spectrum. This article looks at mixed-mode crack growth in epoxy bonded CFRP joints in standard and impact fatigue. It is shown that the back-face strain technique can be used to monitor cracking in lap-strap joints (LSJs) and piezo strain gauges can be used to measure the strain response of impacted samples. It is seen that there is significant variation in the failure modes seen in the samples and that the crack propagation rate is highly dependent on the fracture mode. Furthermore, it is found that the crack propagation rate is higher in impact fatigue than in standard fatigue even when the maximum load is significantly lower.

I. A. Ashcroft · J. P. Casas-Rodriguez ·
V. V. Silberschmidt (✉)
Wolfson School of Mechanical and Manufacturing Engineering,
Loughborough University, Leicestershire LE11 3TU, UK
e-mail: V.Silberschmidt@lboro.ac.uk

Introduction

High-performance fibre-reinforced polymer composites (FRPs) are now well established in many applications such as military aircraft, high-speed marine vessels and sports equipment. Increasing usage is also being found in civil aircraft, automotive and building applications. The original reason for using these materials was the high-specific strength and stiffness; however, other potential advantages include reparability, insulating properties, corrosion resistance, suitability for stealth applications and fatigue resistance. In fact, the good resistance of FRPs to fatigue lead to an early design philosophy based on quasi-static strength alone. However, with further research and increased studies of components after extended periods in service, it is now recognised that fatigue is potentially damaging to composites and hence is worthy of serious study. Furthermore, fatigue is also linked with two of the main drawbacks of these materials, namely, sub-surface damage initiation making it difficult to detect, and, second, possibility of the transfer from stable to unstable crack growth at short crack lengths. Together these two characteristics can mean that the first sign of fatigue damage can be complete failure of the structure. This has lead to research into the fatigue of composites, including the fatigue propagation of sub-surface cracks caused by low-energy impact, such as the classic scenario of the dropped tool during maintenance work [1–3]. Most of this research work has been conducted using simple constant amplitude, sinusoidal waveforms or in some cases simplified versions of load spectra taken from experimental measure using techniques such as the rainflow method. However, the in-service load spectra for structural applications can in some cases contain repetitive low-energy impacts, which are termed *impact fatigue*. This type of loading has received

little attention to date, but has been shown to be damaging to composite materials [4–6].

Composite fabrication methods mean that the number of joints in a structure can often be significantly reduced compared with similar metal structures. However, it is inevitable in all but the simplest applications that composite parts will need to be joined to other parts. In many cases, such as the use of FRP panels in cars, the FRP may have to be joined to a different material, such as aluminium. The most common method of joining is probably mechanical fastening but this is less than ideal for a number of reasons. First, mechanical fastening usually involves drilling a hole in the composite, which will have a detrimental effect on its structural integrity. Furthermore, the site of the mechanical fastener will be a site of high-stress concentration, and potential fretting fatigue can occur between the mechanical fastener and the composite causing further damage. Also, if the structure needs to contain liquid, such as the fuel-holding function of many aircraft wings, then the mechanical fastening is a potential leakage site. Finally, the mechanical fasteners can add significant weight and the fastening process can be expensive, especially if sealing and dressing are required. The obvious alternative to mechanical fasteners is adhesive bonding, and indeed this joining method removes or reduces many of the disadvantages stated above. However, inevitably, certain disadvantages are also associated with adhesive bonding. These include, sensitivity to the manufacturing process (particularly, poor surface preparation), difficulty in detecting poorly bonded areas, environmental sensitivity and a lack of trusted design methods for real in-service conditions. Most of these problems can be overcome, however, and hence there has been a lot of work into the adhesive bonding of composite parts (e.g. [7–12]). The reduction in stress concentration, decrease in damage to the composite and increase in stiffness of bonded joints compared to mechanically fastened joints would indicate improved fatigue resistance, and research has shown that good fatigue resistance can, indeed, be seen in bonded composite joints [13–16]. A significant research effort has also been put into looking at the response of bonded joints to impact loads [17–21], however relatively little work has been published to date on the impact fatigue of bonded composite joints, even though it has been shown that impact fatigue is highly detrimental to bonded joints [22, 23]. In [24] the impact-fatigue behaviour of bonded epoxy-CFRP lap-strap joints was compared to the behaviour of the same joints subjected to non-impact, constant amplitude sinusoidal loading (i.e. standard fatigue). It is shown that the impact fatigue is significantly more damaging to the joints than the standard fatigue. The fracture surfaces for the two types of loading were seen to be quite different, with the impact fatigued joints showing less uniformity and more signs of brittle fracture. The response of similar joints to fatigue spectra incorporating short blocks of impact fatigue in a standard fatigue spectrum has also been reported [25]. It was seen that the incorporation of the impact-fatigue blocks significantly changed the dynamics and mechanisms of crack growth in the joints, resulting in a greatly decreased fatigue life.

In this article, crack growth in standard and impact fatigue of bonded epoxy-CFRP lap-strap joints is investigated. The back-face strain technique is explored as a means of in-situ monitoring of damage in the joints as well as measuring transient strains in the impact fatigued lap-strap joints (LSJs) for the first time. An effort is also made to correlate crack growth with various fracture parameters as a means of developing predictive fatigue crack growth laws.

Experimental

Sample preparation

Samples were manufactured by adhesively bonding cured carbon fibre reinforced polymer (CFRP) panels. This is known as secondary bonding and is distinguished from co-bonding and co-curing, in which the adhesive and CFRP are cured together. The advantage of secondary bonding is that different (optimum) curing cycles can be used for the adhesive and CFRP and that distortion of the CFRP in the joint area during curing can be avoided. There is also potentially greater freedom in the manufacturing process as well as cost savings due to a possibility to make parts in smaller assemblies. However, the obvious disadvantages are the time and cost penalties of replacing a single process with two.

The CFRP pre-preg used in this work was nominally 0.125 mm thick with 60vol% of unidirectional T800 fibres in a Rigidite 5245C matrix from Cytec Ltd. A multidirectional (MD) lay-up scheme of $[(0/-45/+45/0)_2]_S$ was used to manufacture panels 2 mm thick that were cured for 2 h at 182 °C with an initial autoclave pressure of approximately 600 kN/m^2. The elastic properties of the cured panels are given in Table 1. The adhesive used was Hysol Dexter's EA9628, which is a rubber toughened single part epoxy film adhesive of 0.2-mm nominal thickness. The stress–strain behaviour of the adhesive from tensile testing bulk dumbbell samples can be seen in Fig. 1.

Table 1 Elastic properties of T800/5245C composite at room temperature

	E_x (GPa)	E_y (GPa)	G_{xy} (GPa)	ν_{xy}	ν_{xy}
UD	174	9.64	7	0.36	0.02
MD	99.8	28.1	25.7	0.69	0.2

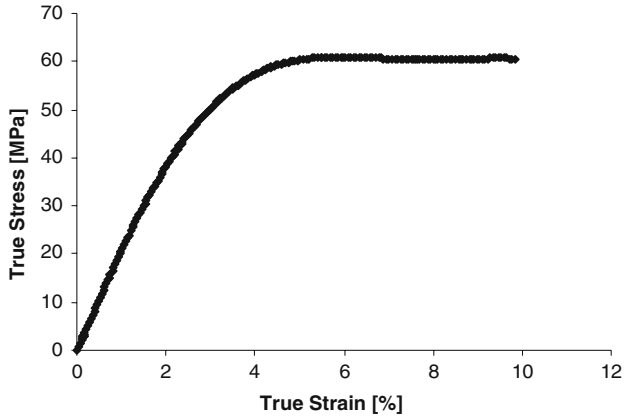

Fig. 1 Stress–strain curve for EA9628 adhesive at room temperature

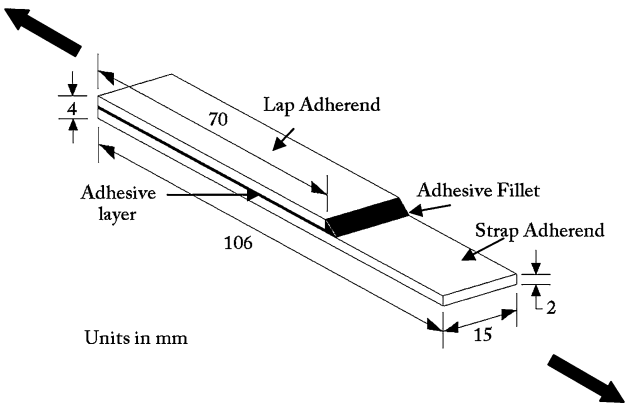

Fig. 2 Dimensions of the lap-strap joint (in mm)

The dimensions of the LSJs used in this investigation are shown in Fig. 2; the thickness of the adherends was 2 mm. This type of joint consists of a strap adherend, which spans the two loading points, and a lap adherend, which terminates at a point along the strap. This geometry behaves very differently to the more commonly used single and double lap joints and is more representative of the kinds of joint used in many structural applications. The CFRP panels were grit blasted and acetone-cleaned prior to bonding. Assembled joints of adhesive and CFRP were cured under pressure in an autoclave for 60 min at 120 °C. The fatigue samples were cut from the bonded panels using a diamond saw. End tabs were bonded to the samples to aid grip in the fatigue tests and to provide load alignment.

Quasi-static and standard fatigue testing

A servo-hydraulic fatigue testing machine with digital control and computer data logging was used in the quasi-static and standard fatigue testing. The quasi-static failure load was calculated as the average of the maximum force reached by two specimens tested at a displacement rate of 0.05 mm/s. Standard fatigue testing was in load control with a maximum load of 7.8 kN, which was approximately 60% of the average quasi-static failure load. A sinusoidal waveform was used with an R-ratio (minimum-to-maximum load) of 0.1 and frequency of 5 Hz. All testing was in ambient laboratory environmental conditions where temperature and relative humidity varied between 18–25 °C and 50–60%, respectively. Thermocouples were placed at various points on the surfaces of the samples in order to investigate any thermo-elastic heating during testing, however, no change in temperature was observed.

In-situ crack growth in the samples was measured by means of a portable optical microscope and digital camera. The edges of the samples were painted white and marked with a scale prior to testing in order to increase the contrast between cracked and non-cracked material and, hence, increase the accuracy of the crack measurements. Back-face strain was also investigated as a means of in-situ measurement of crack length: this is described further in section “Fractography”.

Impact-fatigue testing

The impact-fatigue test used in this work was based on repetitive pendulum impacts using the set-up shown in Fig. 3. The sample was connected to a piezo-electric force transducer at the fixed end, and a striking anvil was

Fig. 3 Schematic of the impact-fatigue test

attached to the free end of the sample. The pendulum was released from a pre-selected initial angle, which corresponded to a potential energy of 1.07 J, and the pendulum impacted the striking anvil at a velocity of 1.5 m/s. This resulted in a tensile force in the sample similar to that seen in the quasi-static and standard fatigue tests, although the boundary conditions were slightly different in that there was more allowable rotation at the loaded end of the sample in the impact fatigue. After each impact the pendulum was automatically caught and returned to the loading position, with the time between impacts being approximately 15 s. Changes in the electrical resistance of the piezo-electric sensor were recorded and the amplified and filtered data was downloaded to a computer as force as a function of time, from which velocity and energy could also be calculated. Measurement of crack growth was made using the method described in next section.

Back-face strain measurement

Two kinds of strain gauge were used in the back-face strain measurements. In the standard fatigue tests a 120 Ω electrical resistance strain gauge with a gauge factor of 2.085 and gauge length of 3 mm was used. In the impact-fatigue tests a piezo-electric strain gauge was used with a gauge factor of 121 and gauge length of 2 mm. The high gauge factor reduces problems of noise in the signal for the low strains in the impact-fatigue tests. Also, the piezo-electric strain gauge can be used at high sampling frequencies (1 GHz in this case) thus allowing strain data to be generated with the same precision as that obtained from the piezo-electric sensor in the sample-holding vice in the impact-fatigue test machine. In the standard fatigue tests, strain gauges were placed on both the strap and lap adherends, in the locations shown in Fig. 4. For the impact fatigue, the strain gauge was only placed on the strap adherend.

Fractography

After testing, the edges and fracture surfaces of each sample were examined with an optical microscope. This was primarily to locate the macro fracture path in the joint and to look for different areas of fracture for further study. Scanning electron microscopy was then used for higher magnification examination of selected fracture surfaces. Specimens were extracted using a diamond saw and gold-coated prior to examination to prevent charging under the electron beam.

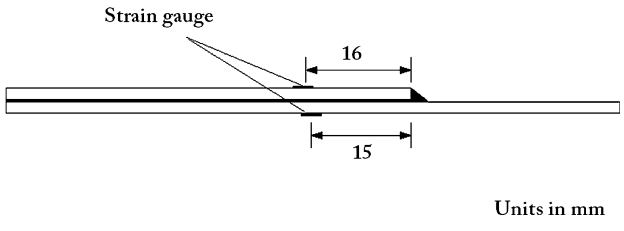

Fig. 4 Positions of the back-face strain gauges

Finite element analysis

The LSJ was modelled in 2-D with the commercial FEA software package MARC-MENTAT (2007-R1) from MSC. The aims of the models were to (a) simulate back-face strain signals for various gauge locations and (b) determine fracture parameters, such as strain energy release rate (G) as a function of crack length and crack path. Four-noded plane strain isoparametric elements with assumed strain interpolation were used as these provided the better calculation of fracture mechanics parameters. However, this meant that a high degree of mesh refinement was necessary to remove a high-mesh dependency in the fracture mechanics parameters determined from the FEA models. The simulated back-face strain measurements were less mesh-sensitive.

The effect of various non-linearities were considered by analysing the model as (i) liner elastic (lin), (ii) geometric non-linear with elastic material properties (gnl) and (iii) geometric and material non-linear (nl). The material properties used in the model were dependent on the type of analysis; in the cases of the linear elastic analysis and the geometric-non-linear analysis both materials were modelled as linear elastic, with the composite having the properties shown in Table 1 and adhesive having elastic modulus and Poisson's ratio of 2.24 GPa and 0.38, respectively. In the case of fully non-linear model, the material was modelled as an elastic-plastic material with properties derived from the stress–strain diagram shown in Fig. 1. The boundary conditions used in all the models are shown in Fig. 5a and the mesh in the overlap region for the model prior to the introduction of a crack can be seen in Fig. 5b.

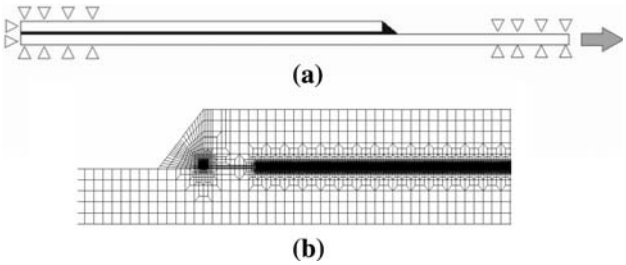

Fig. 5 FEM model: (**a**) boundary conditions; (**b**) overlap area: mesh before cracking

Three locations of cracking were explored in the models, as shown in Fig. 6: (i) a crack in the centre of the adhesive layer (Fig. 6a), (ii) a crack at the interface between the CFRP strap adherend and the adhesive layer (Fig. 6b) and (iii) a crack in the first ply of the strap adherend adjacent to the adhesive layer (Fig. 6c). The three models are aimed at representing the three loci of failure observed experimentally (as discussed in section "Standard fatigue test results"); however, the interface model is rather contentious as the experimental failure was not along a well-defined interface between two materials, and there is the problem of theoretical singularities when determining fracture parameters at bi-material interfaces.

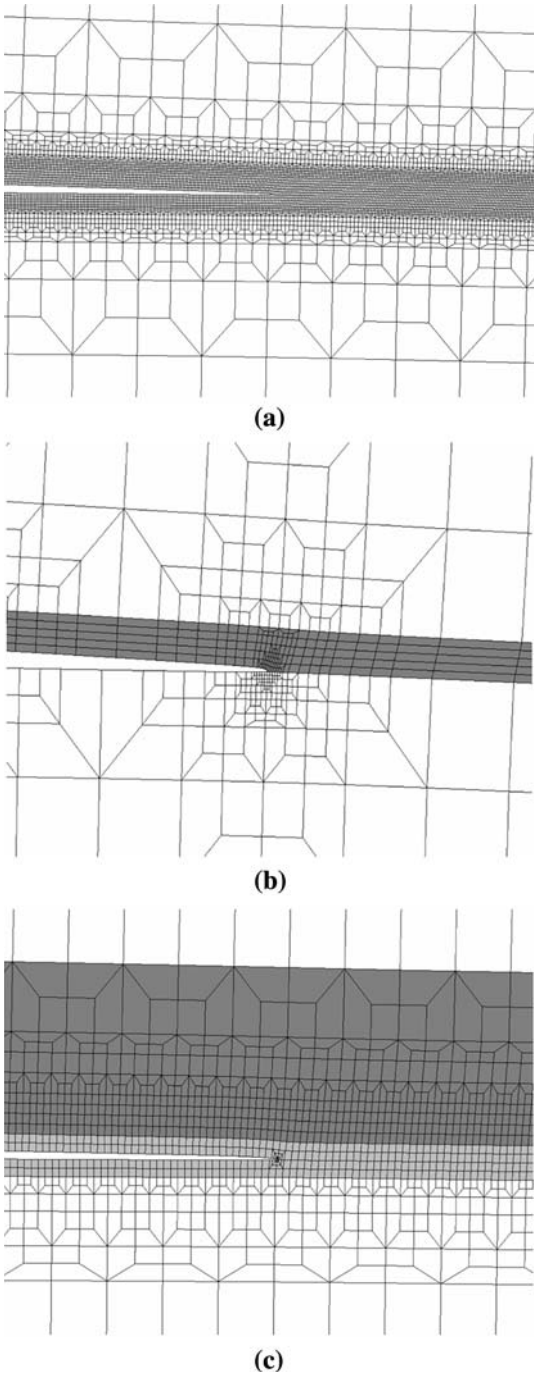

Fig. 6 Meshes with cracks: (**a**) cohesive fracture of adhesive, (**b**) interfacial fracture, (**c**) fracture in first ply of CFRP (adhesive layer in dark grey)

Determination of fracture mechanics parameters

Four methods were used to calculate fracture parameters for the LSJs. The first method used was a simple analytical scheme proposed by Brussat and Chiu [26] (for the rest of this article will be referred to as *the Brussat model*). This model is based on an elastic analysis of an infinite beam, in which the adhesive layer is neglected. The total strain energy release rate (G_T) is defined as the sum of the mode I and mode II contributions (i.e. $G_T = G_I + G_{II}$) and for the Brussat model G_T is termed G_{Brus}, as defined in the following equation:

$$G_{Brus} = \frac{P^2}{2b_N(EA)_2}\left[1 - \frac{(EA)_2}{(EA)_0}\right], \quad (1)$$

where P is the load, b_N is specimen width, $(EA)_2$ is the tensile rigidity of the strap and $(EA)_0$ is the total rigidity (lap + strap). Analysing Eq. 1 it can be seen that G_{Brus} is independent of the crack size. It was further shown in [26] that the ratio G_I/G_{II} for equal thickness adherends using this model is 4/7.

The other three methods of calculating fracture mechanics parameters were based on the finite element models described in section "Finite element analysis". Strain energy release rate was determined from the linear elastic and geometric non-linear models using the virtual crack close (VCC) technique [27]. The respective values are termed G_{lin} and G_{gnl}. For the model with non-linear adhesive properties the J-integral fracture parameter proposed by Rice [28] was determined for three integral paths around the crack tip. A comparison of G and J for cohesive failure in the joints using the various different calculation methods is shown in Fig. 7. Brussat's analytical method predicts a constant value of G with respect to crack length, whereas all the other methods show decreasing values of G/J with crack length, although an initial increase in G to varying degree is seen in the first 10 mm. This can be attributed to the fact that the lap-strap geometry in the FEA model was far from the infinite length assumption in Brussat's analysis, and, hence, end effects are seen along the length of the sample. It can also be seen that the linear FEA analysis shows the greatest variation in G and this is because the geometry is not updated as the sample is loaded. Figure 8 shows the effect of crack location for G_{gnl}. Obviously, there is only a minor effect on the value of G_{gnl},

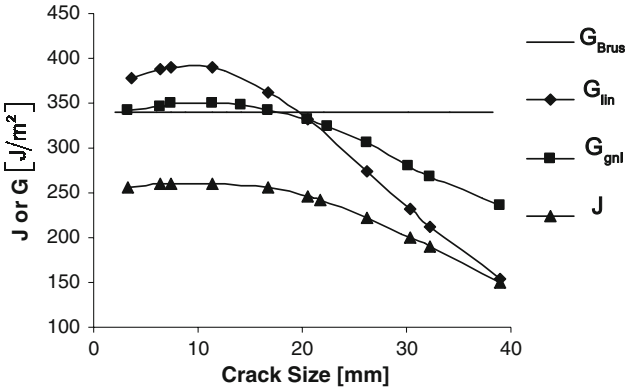

Fig. 7 Comparison of different fracture parameters for cohesive fracture

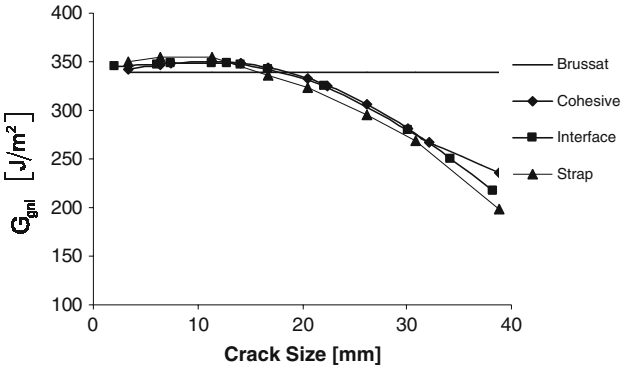

Fig. 8 Comparison of G_{gnl} for different fracture paths

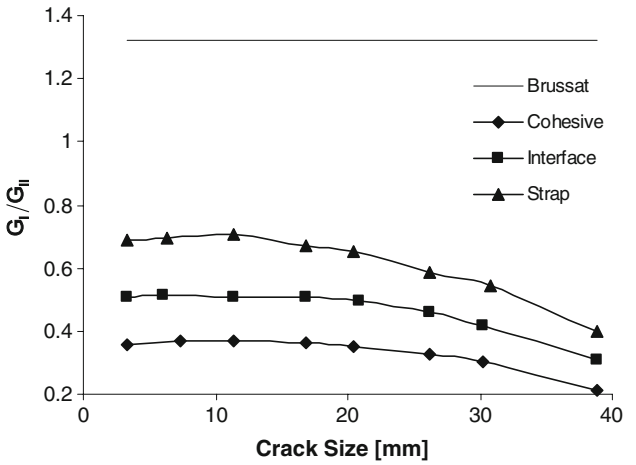

Fig. 9 Comparison of G_{gnl} mode ratio (G_I/G_{II}) for different fracture paths

especially for short cracks. However, Fig. 9 shows that the same cannot be said for mode mix, although, it should be noted that the determination of the individual components of G may be more susceptible to the influence of the singularities at the bi-material interface than for G_T.

Results and discussion

Back-face strain simulations

The results from the FEA back-face strain simulations can be seen in Figs. 10 and 11. Figure 10 shows the results for a strain gauge on the lap adherend back face. Each plot shows how the strain signal varies as the crack grows for a different position on the back face (as measured from the end of the overlap, as shown in Fig. 4). A general pattern is seen, in which the strain decreases steadily until the crack reaches the location along the bondline corresponding to the location of the strain gauge on the back face. At this point there is a dip in the curve and the strain becomes compressive. After the crack has grown beyond this point, the strain gauge on part of the lap adherend is unloaded since the lap is no longer attached to the strap adherend; thus the strain signal becomes zero and is no longer sensitive to crack growth. It can be seen then, that ability to detect crack growth is highly dependent on the position of the strain gauge and the position of the crack. Hence, a different gauge location may be chosen if the aim is to predict the first signs of cracking and if the aim is to monitor crack growth along the length of the sample.

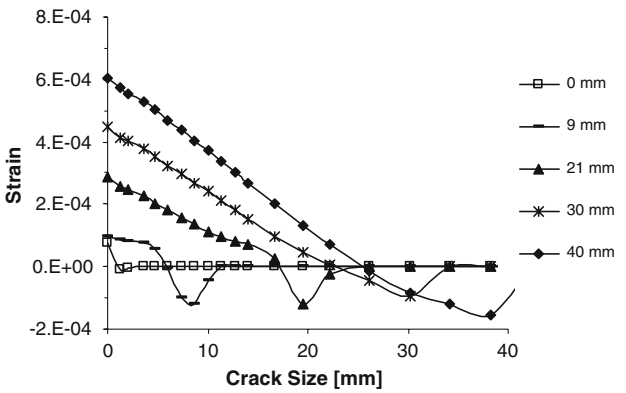

Fig. 10 Back-face strain for different locations on the lap adherend

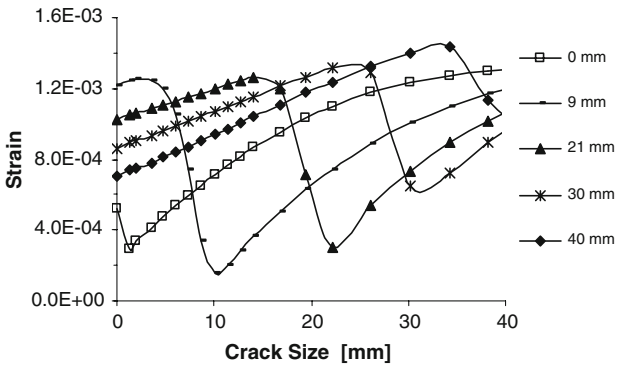

Fig. 11 Back-face strain for different locations on the strap adherend

The results from the FEA simulations with the strain gauge on the strap adherend back face are shown in Fig. 11. Again it can be seen that strain gauge location has a strong effect on crack monitoring. The first thing to note is that the strain levels and the difference between maximum and minimum strains are greater than for the gauge on the lap adherend, which is potentially useful in decreasing experimental scatter, depending on the noise in the experimental strain gauge system. On this adherend the trend is a steady increase in strain as the crack progresses, followed by a large decrease in strain as the crack passes the location of the gauge, after which strain increases again. The big advantage of siting the gauge on the strap adherend is that the gauge can be placed to be most accurate at the site of most interest but is still able to monitor crack growth along the whole length.

Standard fatigue test results

Figure 12 shows a comparison of FEA predicted and experimental BFS plots from the standard fatigue tests. Results with the strain gauge bonded to the back face of the lap adherend at a position of 16 mm from the end of the overlap (shown in Fig. 4) are presented in Fig. 12a. It can be seen that although there is some scatter in the experimental strain gauge reading, there is good agreement between the predicted and experimental results. It justifies that placing a strain gauge at this position provides a good monitor of the crack length until the crack is approximately 20 mm in length, after which the strain gauge is insensitive to further crack growth. Figure 12b shows the results for a strain gauge bonded to the back face of the strap adherend at a distance of 15 mm from the end of the overlap, once more demonstrating good agreement between the predicted and experimental strains. The scatter is reduced in this case, which can be attributed to the higher strains that diminish the effect of noise in the measuring system. This result shows that the back-face strain on the strap adherend can be used to monitor crack length over the length of the sample. However, it should be noted that greatest positional accuracy will be gained from this technique where the strain gradient is highest, i.e. around the position at which the gauge is placed.

The two samples tested in standard fatigue exhibited different failure paths. The first sample failed within the adhesive layer along its entire length, as shown schematically in Fig. 13a. The other sample, however, exhibited a more complex fracture path. Failure initiated in the adhesive fillet at the end of the overlap and progressed through the adhesive for approximately 20 mm. Failure then progressed to the interfacial area between the adhesive and the strap adherend, exhibiting mixed failure in the adhesive and in the top ply of the CFRP strap. After a further 10 mm

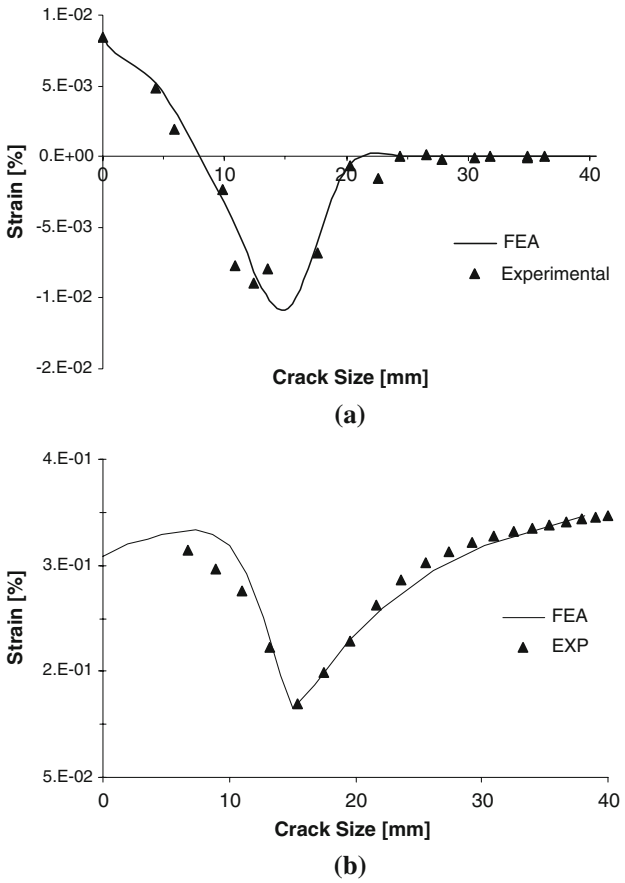

Fig. 12 Comparison between experimental and FEA back-face strains for gauge at 16 mm (**a**) and 15 mm (**b**) from the fillet on the strap adherend

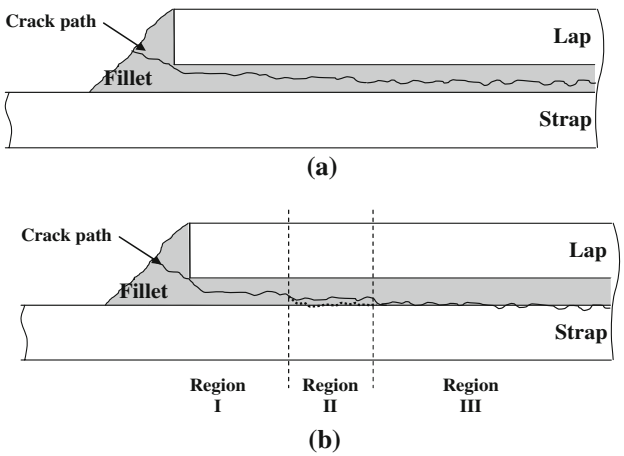

Fig. 13 Crack path schematic: (**a**) cohesive fracture in adhesive; (**b**) mixed fracture path

the fracture was predominantly within the 0 degree ply of the strap adherend adjacent to the adhesive layer. This is shown schematically in Fig. 13b. It should be noted that this was similar to the type of failure noted in the larger samples reported in previous work [24, 29, 30].

The crack growth rate (*da*/*dN*, where *a* is crack length and *N* is number of cycles) as a function of crack length for the two samples tested in standard fatigue can be seen in Fig. 14a. The sample that failed completely cohesively shows a steadily decreasing crack growth rate as crack length increases. This may be expected considering the decrease in *G* with crack length shown in Figs. 7 and 8. The sample with the mixed failure path shows similar results to the cohesive failure sample for the first 15–20 mm, which is not surprising as both samples are failing predominantly in the adhesive in this region. However, once the crack starts to propagate predominantly in the composite there is a sharp increase in the crack growth rate, although this levels as crack length increases further. Figure 14(b) presents the crack growth rate plotted as a function of G_{gnl} for both samples in double logarithmic co-ordinates. The sample with the cohesive failure shows the classic 3 zone fatigue crack growth behaviour [31, 32], with a threshold region at approximately 140 J/m^2 and fast-growth region at approximately 350 J/m^2. In between these two regions is an area, in which log log(*da*/*dN*) is proportional to log*G*. This is known as the *Paris region* as it conforms to the crack growth law proposed by Paris [33]. The following relation presents a modified form of Paris law, in which *G* is used in place of stress intensity factor, *K*:

$$\frac{da}{dN} = C(\Delta G)^n, \tag{2}$$

where ΔG is the strain energy release rate amplitude in the fatigue loading, although, in some cases the maximum strain energy release rate is used as an alternative parameter in Eq. 2. The fatigue crack growth plot for the mixed-mode failure is coincident with the cohesive failure plot at high levels of *G*, where failure is cohesive for both samples. However, as *G* decreases with crack length there is an increase in the rate of crack growth. For a homogeneous type of fracture this would seem a nonsensical result; however, it is perfectly explainable in the mixed failure case. It has already been shown that for this system the fatigue resistance of the CFRP matrix is less than that for the adhesive at room temperature [34], thus crack growth rate in the CFRP would be expected to be higher than that for the adhesive for a given value of *G*. This would result in different fatigue crack growth plots for failure in the adhesive and the CFRP, as shown schematically in Fig. 15. It is thus easy to see from this figure how an increasing crack growth rate with decreasing *G* is obtained as the fracture path moves from the adhesive to the CFRP.

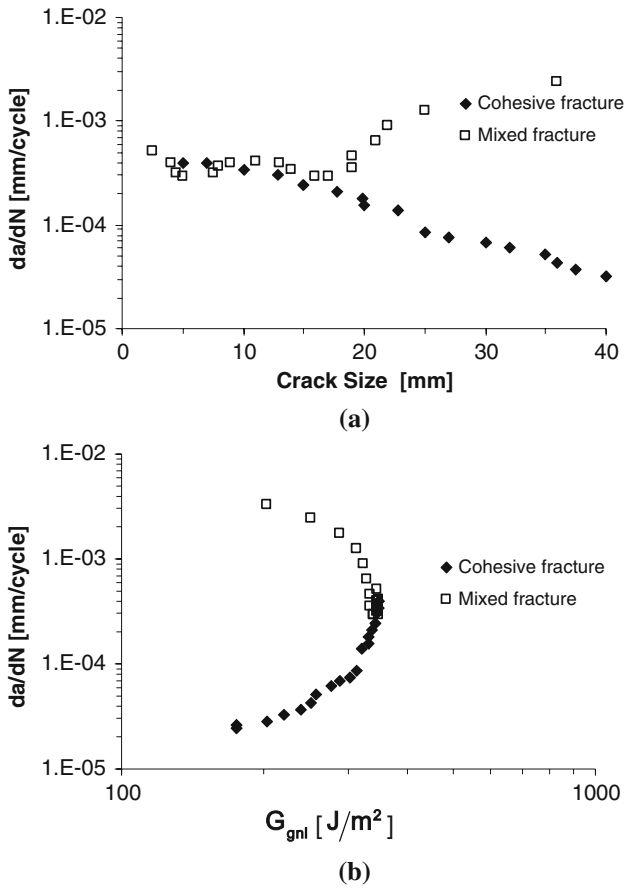

Fig. 14 Crack growth rate in standard fatigue as a function of crack length (**a**) and strain energy release rate (**b**)

Impact-fatigue results

A comparison of the signals from the piezo strain gauge attached to the strap adherend and the piezo load transducer attached to the sample grips for a typical impact are presented in Fig. 16. It is obvious that the load and strain signals generally show good correlation. The force and strain responses are dominated by an initial peak of approximately 1 ms, with subsequent peaks of much smaller amplitude. It should be noted that the maximum load in the impact fatigue is considerably less than that in the standard fatigue testing. There is no obvious time lag between the two signals or difference in damping behaviour, however, there are small differences in the two signal

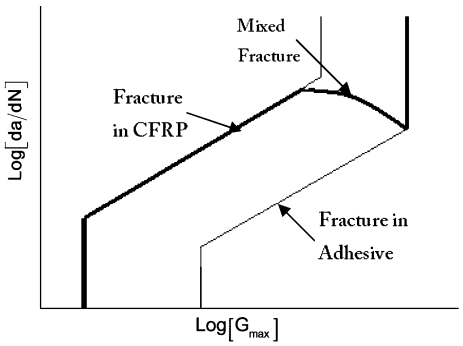

Fig. 15 Mixed-mode fracture model

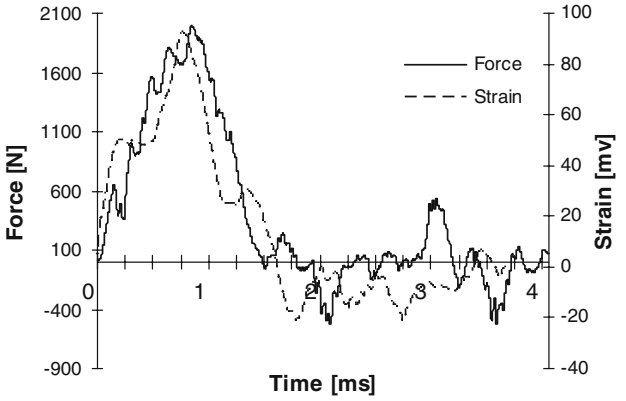

Fig. 16 Force and strain results for typical impact in impact fatigue

paths, which are likely to be a consequence of scatter rather than systematic. It should be noted that similar experiments with standard electrical resistance strain gauges were not able to generate usable results because of the high noise and lower frequency response.

The evolution of the back-face strain signal as the crack grows in impact fatigue (Fig. 17a) shows that the signal varies as the crack progresses. The centre of the gauge is at 15 mm from the overlap, and it can be seen that there is a reduction in the peak load as the crack reaches the position of the gauge. It can also noticeable that once the crack has passed the position of the gauge there is a significant negative strain in the strap after the first tensile peak. Figure 17b demonstrates variation in the peak strain with the crack progresses. This plot is not quite so well defined as that shown in Fig. 12b for standard fatigue, but it is clear that the gauge shows the characteristic decrease in strain as the crack approaches the position of the gauge and there are also signs of the predicted increase in strain as the crack progresses beyond the position of the gauge. In order to better understand this response, dynamic FEA models will be used to create calculated back-face strain plots from impact-fatigue tests in future work.

The impact-fatigue samples tended to exhibit complex mixed-mode fractures, similar to that shown schematically in Fig. 13b. However, the transition from Region I to Region II was much earlier in those samples, at about 2–7 mm. The crack growth rate for the impact-fatigue tests is shown in Fig. 18 as a function of crack length. First, it can be seen that fracture rates tend to be higher than those seen in standard fatigue, as shown in Fig. 14a, even though the maximum loads in impact fatigue are less than a quarter those in standard fatigue. This can be partly attributed to the fact that the switch from failure in the adhesive to failure in the CFRP, which is associated with an increase in fracture rate, occurs much earlier. It is also seen that in a number of the samples there is a general trend of decreasing rate with increasing length, consistent with a decreasing G under constant load. It should be although noted that the decreasing G predicted in

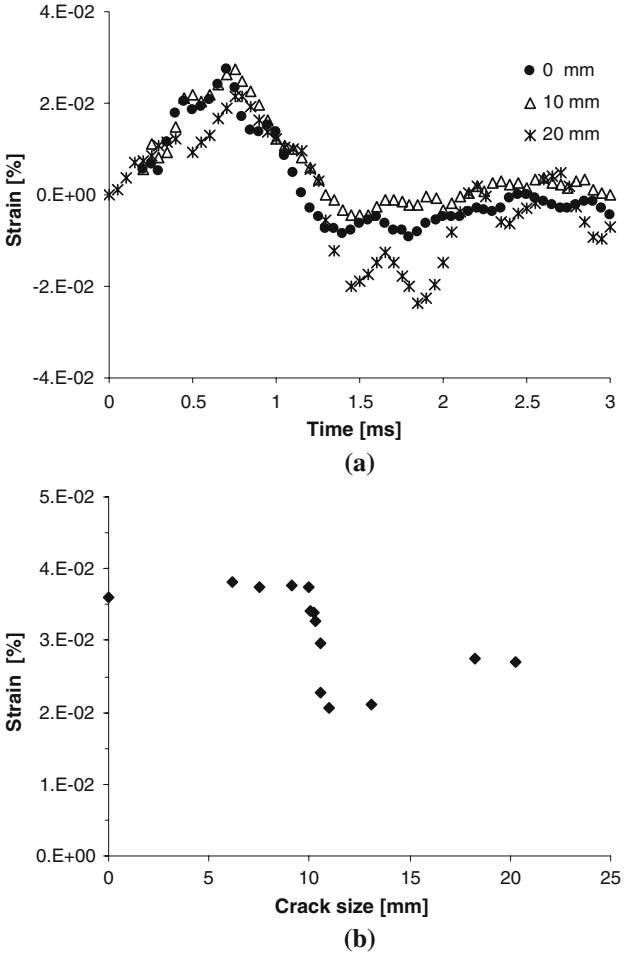

Fig. 17 Impact fatigue: (**a**) change in back-face strain with crack length; (**b**) maximum strain as a function of crack length

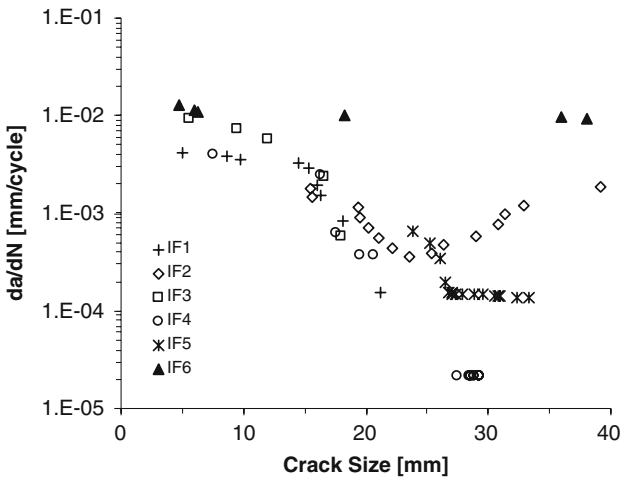

Fig. 18 Fatigue crack growth rate as a function of crack length in impact fatigue

Figs. 7–9 was from a static analysis, and a better understanding of the fracture dynamics may be gained from the dynamic FEA to be carried out in future work. Figure 18 also

demonstrates a significant degree of sample-to-samples variability, which is a feature of impact fatigue of these samples and can be attributed to the multitude of damage mechanisms and the geometrical and material variations in the samples. Of particular note are IF6, which demonstrates a consistently high crack growth rate, and IF2, which shows an increasing rate after approximately 25 mm of crack growth. The change in slope in IF2 can be attributed to an additional fracture mechanism, delamination between 0° and 45° plies in the strap, appearing at this point. In IF6 it was observed with scanning electron microscopy that there were little signs of the cavitations of the rubber toughening particles in the adhesive seen in some of the other fracture surfaces.

Conclusions

It can be concluded from this work that the back-face strain technique can be used to monitor crack growth in LSJs in both standard and impact fatigue. However, the location of the gauge is critical, with the best location being on the strap adherend and placed along the length at the position, in which the greatest accuracy is required. Ideally, a series of crack gauges along the length of the strap should be used. It is also found that in impact a piezo strain gauge should be used rather than a standard electrical resistance gauge, both for noise suppression and to achieve the high sampling rates needed to characterise the strain response under high-rate conditions.

In both standard and impact-fatigue testing, it was found that complex crack paths could develop introducing variability in the crack growth behaviour of similar joints subjected to the same loading. This can be attributed to the complex and variable microstructure of both the adhesive and CFRP, the many and complex micro mechanisms of damage and failure in the joints and the significance of small geometrical, material and flaw variations in determining the crack path. Since the crack growth rate is highly dependent on the mode of fracture this means that a high degree of scatter in crack growth behaviour is inevitable, and this seems to be particularly the case in the dynamic conditions of fracture in impact fatigue.

Acknowledgement The authors are very grateful for a partial financial support by the Royal Society within the framework of its International Joint Projects scheme.

References

1. Cantwell W, Curtis PT, Morton J (1983) Composites 14:301. doi:10.1016/0010-4361(83)90020-4
2. Ramkumar RL (1983) Effect of low-velocity impact damage on the fatigue behaviour of graphite/epoxy laminates. In: O'Brien TK (ed) Long term behaviour of composites, ASTM STP 813, ASTM, Philadelphia, pp 116–135
3. Clark G, Saunders DS (1991) Mater Forum 15:333
4. Ray D, Sarkar BK, Bose NR (2002) Comp A 33:233. doi:10.1016/S1359-835X(01)00096-3
5. Khan B, Rao RMVGK, Venkataraman N (1994) J Reinf Plast Comp 14:1150
6. Sinmmazçelik T, Armağan A (2006) J Mater Sci A 41(19):6237. doi:10.1007/s10853-006-0720-5
7. Davies P (2005) Bonding of composites. In: Adams RD (ed) Adhesive bonding: science, technology and applications. Woodhead Publishing, Cambridge, pp 279–301
8. Tong L, Steven GP (1999) Analysis and design of structural bonded joints. Kluwer Academic Publishing, London
9. Adams RD, Comyn J, Wake WC (1997) Structural adhesive joints in engineering, 2nd edn. Chapman and Hall, London
10. Hart-Smith LJ (2002) J Compos Tech Res 24:133
11. Ashcroft IA, Hughes DJ, Shaw SJ (2000) Assembly Autom 20:150. doi:10.1108/01445150010321797
12. Ashcroft IA, Hughes DJ, Shaw SJ (2001) Int J Adhes Adhes 21:87. doi:10.1016/S0143-7496(00)00038-5
13. Schön J, Starikov R (2000) Fatigue of joints in composites structures. In: Harris B (ed) Fatigue in composites. Woodhead Publishing Limited, Cambridge, pp 621–643
14. Mall S, Ramamurthy G, Rezaizdeh MA (1987) Compos Struct 8:31. doi:10.1016/0263-8223(87)90014-6
15. Ashcroft IA, Abdel Wahab MM, Crocombe AD, Hughes DJ, Shaw SJ (2001) J Adhesion 75:61. doi:10.1080/00218460108029594
16. Ashcroft IA (2004) J Strain Anal 39:707. doi:10.1243/0309324042379239
17. Sato C (2005) Impact behaviour of adhesively bonded joints. In: Adams RD (ed) Adhesive bonding: science, technology and applications. Woodhead Publishing, Cambridge, pp 164–187
18. Beevers A, Ellis MD (1984) Int J Adhes Adhes 4(1):13. doi:10.1016/0143-7496(84)90055-1
19. Kihara K, Isono H, Yamabe H, Sugibayashi T (2003) Int J Adhes Adhes 23:253. doi:10.1016/S0143-7496(03)00004-6
20. Adams RD, Harris JA (1996) Int J Adhes Adhes 16:61. doi:10.1016/0143-7496(95)00050-X
21. Yokoyama T (2003) J Strain Anal 38(3):233. doi:10.1243/030932403765310563
22. Usui Y, Sakata O (1984) Jpn Soc Proc Eng 18(3):213
23. Casas-Rodriguez JP, Ashcroft IA, Silberschmidt VV (2007) Int J Sound Vib 308:467. doi:10.1016/j.jsv.2007.03.088
24. Casas-Rodriguez JP, Ashcroft IA, Silberschmidt VV (2007) Compos Sci Technol. doi:10.1016/j.compscitech.2008.04.030
25. Casas-Rodriguez JP, Ashcroft IA, Silberschmidt VV (2008) Compos Sci Technol. doi:10.1016/j.compscitech.2007.11.006
26. Brussat TR, Chiu ST, Mostvoy S (1977) Fracture mechanics for structural adhesive bonds—final report, AFML-TR-77-163, Air Force Materials Laboratory, Wright Patterson Air Force Base, Dayton, OH
27. Sethuraman R, Maiti SK (1988) Eng Fract Mech 30:227. doi:10.1016/0013-7944(88)90226-3
28. Rice JR (1968) J Appl Mech 35:379
29. Ashcroft IA, Abdel Wahab MM, Crocombe AD, Hughes DJ, Shaw SJ (2001) Compos Part A 32:45. doi:10.1016/S1359-835X(00)00131-7
30. Abdel Wahab MM, Ashcroft IA, Crocombe AD, Hughes DJ, Shaw SJ (2001) Compos Part A 32:59. doi:10.1016/S1359-835X(00)00132-9
31. Ashcroft IA (2005) Fatigue. In: Adams RD (ed) Adhesive bonding: science, technology and applications. Woodhead Publishing, Cambridge, pp 209–237
32. Schijve J (2001) Fatigue of structures and materials. Kluwer Academic, London
33. Paris PC, Erdogan F (1963) Trans ASME D 85:528
34. Ashcroft IA, Shaw SJ (2002) Int J Adhes Adhes 22:151. doi:10.1016/S0143-7496(01)00050-1